Variable Gain DNA Nanostructure Charge Amplifiers for Biosensing

Jacob M. Majikes[1], Seulki Cho[1], Thomas E. Cleveland IV[2,3], J. Alexander Liddle[1] and Arvind Balijepalli[1]

[1]Microsystems and Nanotechnology Division
National Institute of Standards and Technology, Gaithersburg MD 20899
[2]Biomolecular Measurement Division,
National Institute of Standards and Technology,
Gaithersburg, MD 20899
[3]Institute for Bioscience and Biotechnology Research,
University of Maryland, Rockville, MD 20850

e-mail: arvind.balijepalli@nist.gov

Contents

S1: DNA Nanostructure Size and Design

The DNA nanostructure, as discussed in the main text, was designed to be approximately ≈ 69 nm long, ≈ 6 nm tall, and ≈ 18 nm wide. The structure used here is consistent with the one labeled in the cited work[1] as nDFS.B. The lock motif was modified, as were the 9 positions which anchor the structure to the electrode.

It should be noted that the hinge design is on the square lattice (helices are connected at π/2 rad (90 ˚) angles. As dsDNA is only relaxed at a helicity of 10.5 nucleotides per full rotation, and connection points can only occur between helices at integer numbers of nucleotides, 3D structures built in this way are inherently strained. As seen in Fig. 1 of the main text, this strain is compensated by applying a slight torque on the hinge arms.

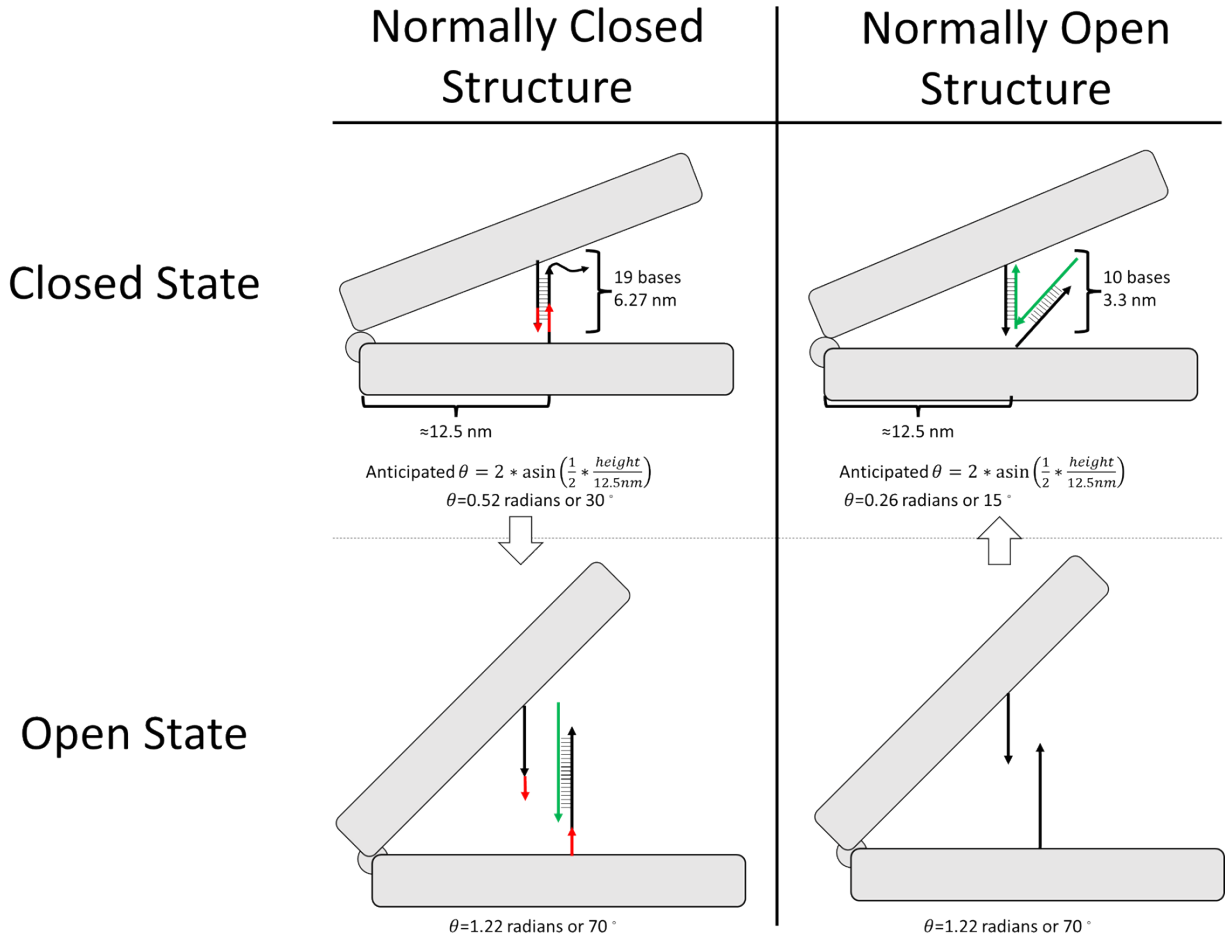

Fig. S1.1: Schematics of the normally open and normally closed structures, the hybridization of their lock motifs in their open and closed states, and the estimated angle those lock motifs should enforce.

Relevant strand sequences

Base Analyte	TTATGTGACCGACGAGACTA
Analyte_W/Toe	AGTTC TTATGTGACCGACGAGACTA
New Analyte Complement	TAGTCTCGTCGGTCACATAA

Thiolated Analyte Complement Strand (for ssDNA hybridization control)	/5DTPA/TTTACCGGAAGCAAACTGCTTCAAAGCG
Unmodified Top Lock staple	ATAAGCGGAATTATCATCATATTTTAAATACCGTTC
Unmodified Bottom Lock staple	AAGATGATGAAACAAATCAATATAAGAATCCTTT

Where Analyte_W/Toe was used to allow for preliminary strand exchange experiments. The Unmodified Top Lock staple and Unmodified Bottom Lock staple sequences correspond to CSBottom and CSTop.[1]
These sequences were used to generate the lock motif sequences, given below.

Red indicates the toehold sequence for strand displacement, green indicates spacer bases, Blue indicates the respective base sequence.

Default Closed Structure		Default Open Structure	
Sticky Seq. Top	TTGACCGACGAGACTAGTG	Sticky Seq. Top	TAGTCTCGTC
Sticky Seq. Bottom	TCACTAGTCTCGTCGGTCACATAA	Sticky Seq. Bottom	GGTCACATAA
Closed Top	ATAAGCGGAATTATCATCATATTTTAAATACCGTTCTTGACCGACGAGACTAGTG	Open Top	ATAAGCGGAATTATCATCATATTTTAAATACCGTTCTAGTCTCGTC
Closed Bottom	AAGATGATGAAACAAATCAATATAAGAATCCTTTTCACTAGTCTCGTCGGTCACATAA	Open Bottom	AAGATGATGAAACAAATCAATATAAGAATCCTTTGGTCACATAA

The anchor strands used in the cited work were modified to remove the ssDNA spacer between the dsDNA stilts and the DNA nanostructure.

Name	Sequence
Surface1	TTCAGAGGCAGGAAACAAAAAATAACGGCTTAATTGCGCTTTGAAGCAGTTTGCTTCCGGT
Surface2	GTTTTATAACTAACAAAGAAAGAAACAAGGTAATTGCGCTTTGAAGCAGTTTGCTTCCGGT
Surface3	AGAATCGCATCTTACCAACGCTAATTGAAGCCCGCTTTGAAGCAGTTTGCTTCCGGT
Surface4	TATCATATTATTATTTATCCCAATAAGGCTTACGCTTTGAAGCAGTTTGCTTCCGGT
Surface5	AGCGCTAACCTTTACAGAGAGAATAAGCCGTTCGCTTTGAAGCAGTTTGCTTCCGGT
Surface6	TATTACGCAATACCGACCGTGTGACTGTTTAGCGCTTTGAAGCAGTTTGCTTCCGGT
Surface7	GCATTTTCGGTCATAGTCAGAGCCGCCAAACGAAAAGACCCGCTTTGAAGCAGTTTGCTTCCGGT
Surface8	CAGTAGCGCATATGGTTTACCAGCAGACTCCTCGCTTTGAAGCAGTTTGCTTCCGGT
Surface9	GCACCATTATATTGACGGAAATTAGTTACCAGCGCTTTGAAGCAGTTTGCTTCCGGT
Thiol Anchor	/5DTPA/TTTACCGGAAGCAAACTGCTTCAAAGCG

S2: Electrochemical Measurements Methods and Measurements

Electrochemical impedance spectroscopy (EIS) measurements modeled using a Randles circuit[2] (Fig. S2.1A) that represents the solution resistance (*Rs*), the resistance of the electrode interface (*Rp*) and a constant phase element (CPE). The impedance, *Z*, of the CPE was of the form $Z = 1/C_p(j\,\omega)^p$, where *Cp* is the interface capacitance, p is an exponent that models non-homogeneity in the system and ω is the angular frequency. were performed for ssDNA (Fig. S2.1B), and the *normally closed* (Fig. S2.1C) and *normally open* (Fig. S2.1D) DNA nanostructures. A complete table of the fit parameters for the model in Fig. S2.1A are shown in Table S2.1.

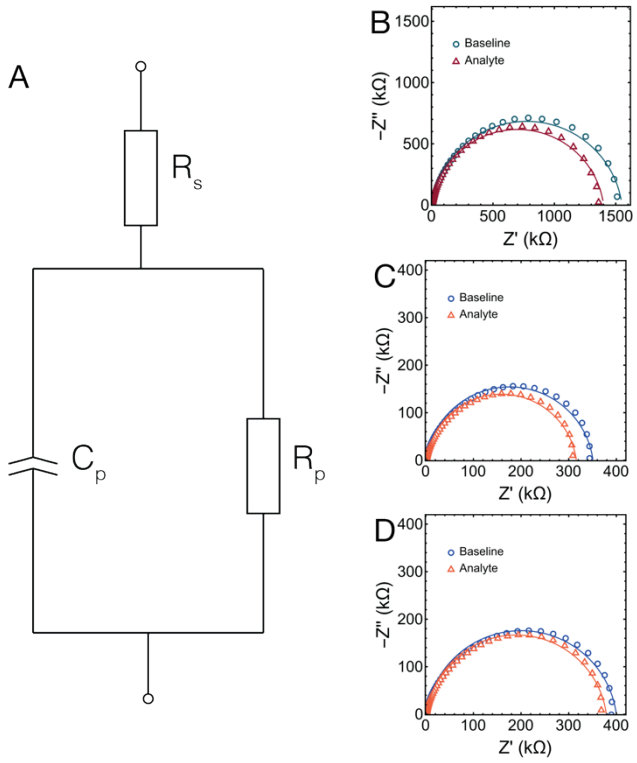

Fig. S2.1: (A) Equivalent circuit diagram used to model electrochemical impedance spectroscopy (EIS) measurements. (B) EIS measurements of ssDNA (*green*) and upon adding 1 nmol/L of complementary analyte (*red*). (C) EIS measurements of the *normally closed* DNA nanostructures (*blue*) and upon adding 1 nmol/L of complementary analyte (*orange*). (D) EIS measurements of the *normally open* DNA nanostructures (*blue*) and upon adding 1 nmol/L of complementary analyte (*orange*).

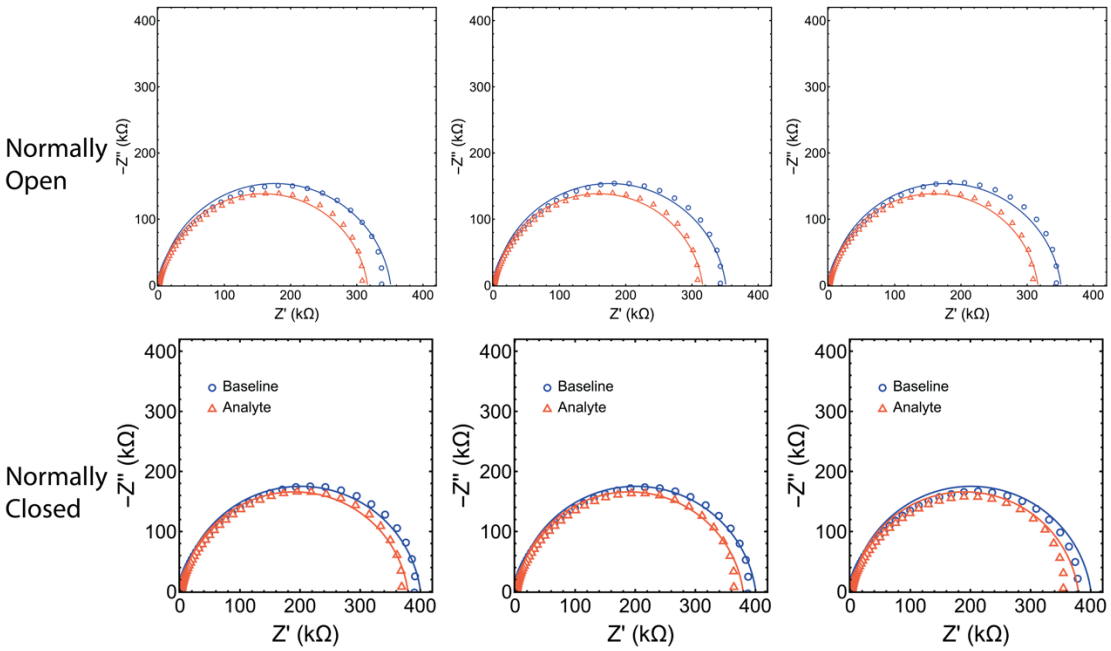

Fig. S2.2: Independent electrochemical impedance spectroscopy (EIS) measurements of baseline and 1 nmol/L (nM) analyte for (*top*) normally open and (*bottom*) normally closed structures.

The ssDNA used in Fig. S2.1 B, as well as in Fig. 3D of the main text was that of the thiolated analyte complement strand, given in the previous section.

Table S2.1: Fit parameters for the circuit in Fig. S2.1

	Rs (Ω)	**Rp (kΩ)**	**Cp (nF)**	**n**
ssDNA Baseline	918±5	1551±12	38.7±0.3	0.89±0.00
ssDNA Analyte (1 nmol/L)	948±0.3	1360±17	41.4±0.6	0.90±0.00
Normally Closed DNA Nanostructure Baseline	898±2	335±4	119±1	0.92±0.00
Normally Closed DNA Nanostructure Analyte (1 nmol/L)	726±2	307±1	143±2	0.91±0.00
Normally Open DNA Nanostructure Baseline	936±1	375±7	99±1	0.92±0.00
Normally Open DNA Nanostructure Analyte (1 nmol/L)	963±1	358±7	117±3	0.91±0.00

S3: Electrical Double Layer and Electrode Passivation Corrections to DNA nanostructure Capacitance

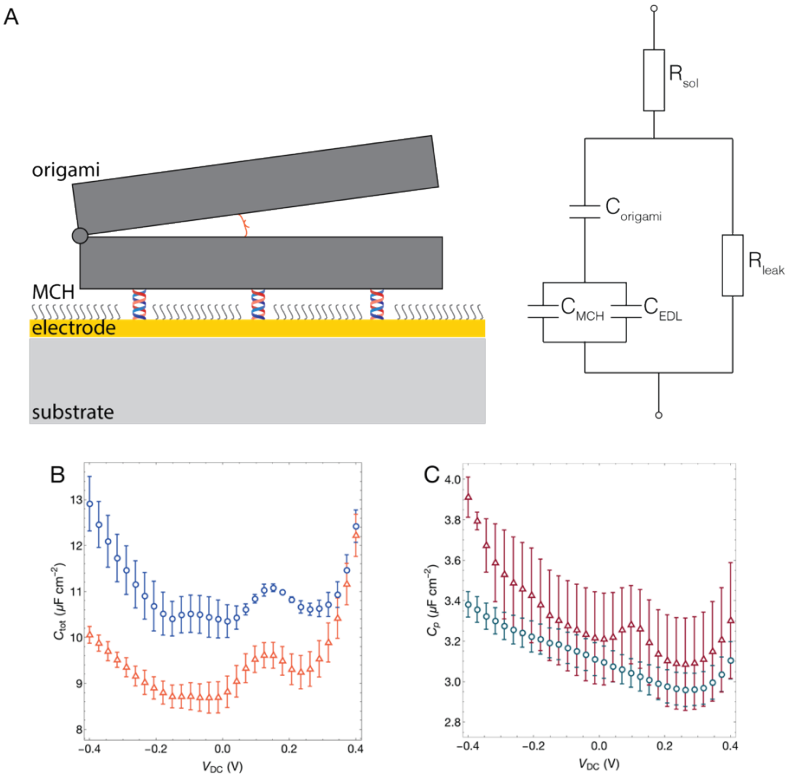

Fig S3.1: (A) (*left*) Schematic representation of the DNA nanostructures anchored to a gold electrode with the unreacted gold surface passivated with 6-mercapto-1-hexanol (MCH) and (*right*) the equivalent circuit model for this system. (B) Capacitance measurements of the *normally closed* (*blue*) and *normally open* (*orange*) cases as a function of a DC bias potential (V_{DC}). (C) Capacitance measurements of single stranded DNA probes on a gold surface (*green*) and upon adding 1 nmol/L of analyte with a complementary sequence to the probes (*red*) as a function of V_{DC}.

Fig. S3.1A (*left*) shows a schematic of the DNA nanostructures measurement on a gold electrode. Each DNA nanostructure structure is attached to the gold surface with 9 double stranded DNA (dsDNA) strands and the unreacted gold surface is passivated with 6-mercapto-1-hexanol (MCH). The system is modeled with an equivalent electrochemical circuit[3] shown in Fig. S3.1A (*right*). The effective capacitance (C_{tot}) of the system can be separated into its constituent elements shown in the figure and represented by the equation,

$$\frac{1}{C_{tot}} = \frac{1}{C_{structure}} + \frac{1}{C_m}, \qquad \text{(S3.1)}$$

where $C_{structure}$ is the capacitance of the DNA nanostructures and C_m=C_{MCH}+C_{EDL} is the effective capacitance of the passivation surface that includes the capacitance of the MCH layer (C_{MCH}) and that of the electrical double layer (C_{EDL}) of unpassivated electrode surface.[4,5] We estimate the effective value of C_m as a function of the applied DC bias relative to an AgCl reference electrode (V_{DC}) by measuring a surface functionalized with MCH but without the DNA nanostructures. By using Eq. S3.1, we then isolate the contribution of $C_{structure}$ from the overall capacitance in Fig. S3.

S4. DNA Nanostructure Capacitance Model as a Function of Opening Angle

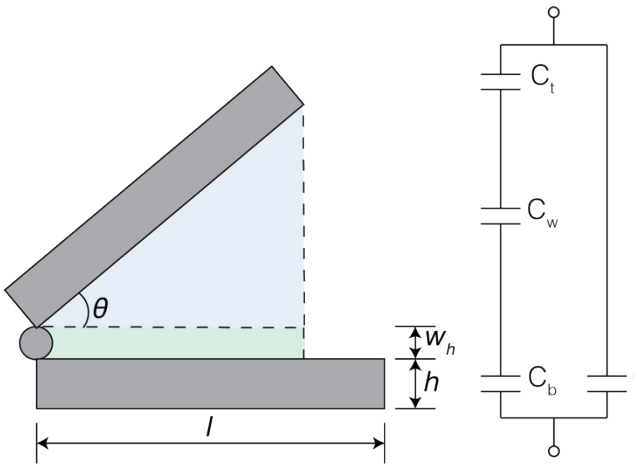

Fig. S4.1: Schematic and equivalent circuit model of a DNA nanostructures

To model the capacitance of the DNA nanostructure as a function of hinge angle, the capacitance was divided into four components. The bottom arm of the DNA nanostructure that is under the projected length of the top arm is modeled by Eq. S4.1, where ε_0 is the vacuum permittivity, ε is the dielectric constant, l is the hinge length, d is the hinge depth, h is the height of each hinge, and θ is the angle of the hinge. The dielectric constant of the DNA nanostructures is assumed to be equal to that of the buffer solution since the structure is liquid filled.

While this arm is immobile, its contribution to the total capacitance is related to the amount of overlap with the top arm and is a function of θ. The contribution of the bottom arm that is not under the shadow of the top arm is given later by Eq. S4.4.

$$C_b = \frac{\varepsilon\varepsilon_0 l\, d\, cos(\theta)}{h}. \tag{S4.1}$$

The water layer between the two arms of the DNA nanostructure changes as a function of θ as seen by the equation below,

$$C_w = \varepsilon\varepsilon_0 \int_0^{l\,cos(\theta)} \frac{d}{h + x\,sin(\theta)} dx = \varepsilon\varepsilon_0 d\, csc(\theta)\left(\ln\left(w_h + l\cos(\theta)\sin(\theta)\right) - ln(w_h)\right), \tag{S4.2}$$

where, w_h is the length of the spacer bases which connect the hinge halves.

The capacitance of the mobile top arm of the DNA nanostructure is given by,

$$C_t = \varepsilon\varepsilon_0 \frac{l\, cos(\theta)}{h\, sin(\theta)}, \tag{S4.3}$$

Finally, the portion of the bottom arm that is exposed to solution as the top arm actuates, while ignoring the contribution from the electrical double layer, is given by,

$$C_{b^-} = \varepsilon\varepsilon_0 \frac{l\, d(1 - \cos(\theta))}{h}, \tag{S4.4}$$

Eq. S4.1 – S4.2 can be combined to obtain the final expression in Eq. 1 by using,

$$C_t(\theta) = \left(\frac{1}{C_b} + \frac{1}{C_w} + \frac{1}{C_t}\right)^{-1} + C_{b^-} \quad \text{(S4.5)}$$

S5: Hypothesized Tether or Stilt Behavior

The original hinge origami design utilized 9 identical sticky end extensions which would hybridize to 9 copies of a thiolated sequence. In the cited work there was a large ssDNA spacer on these stilts which we removed after preliminary results indicating that this obscured the capacitance data by allowing the structure to be too mobile.

For the nanostructures in this manuscript the 9 anchor positions were comprised of 25 nucleotides of dsDNA, approximately 8.3 nm in length. These could be considered freely jointed at both the gold surface and the origami, and as such, could be expected to collapse as shown in fig. S5.1. The similarity in the peak in capacitance as a function of DC bias between the hinge nanostructure and plain dsDNA would support that at 0.15V the dsDNA is forced to lie flat on the electrode surface.

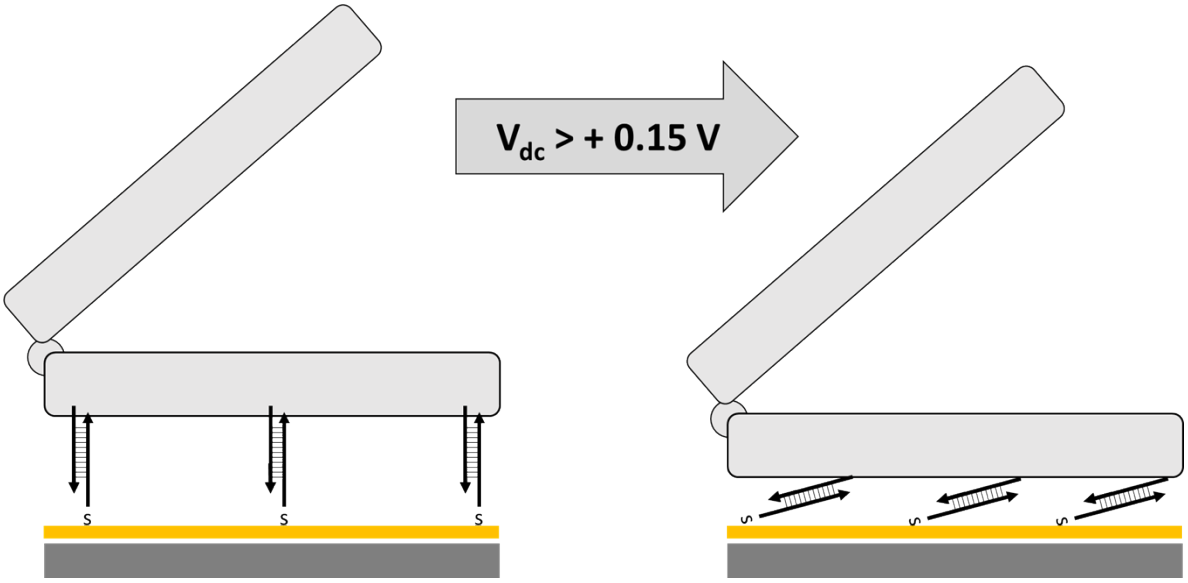

Fig. S5.1: Schematic of the 25 base anchor strands, and how they could be forced to lie collectively flat on the surface of the electrode by an applied positive voltage.

S6: AFM images of Hinge DNA Nanostructures

AFM was found to be an unsatisfying method to characterize the hinge structure, as under typical conditions of liquid imaging mica in 12.5 mM Mg^{2+} the structures were sufficiently tall and sufficiently weakly bound o the surface to result in poor image quality.

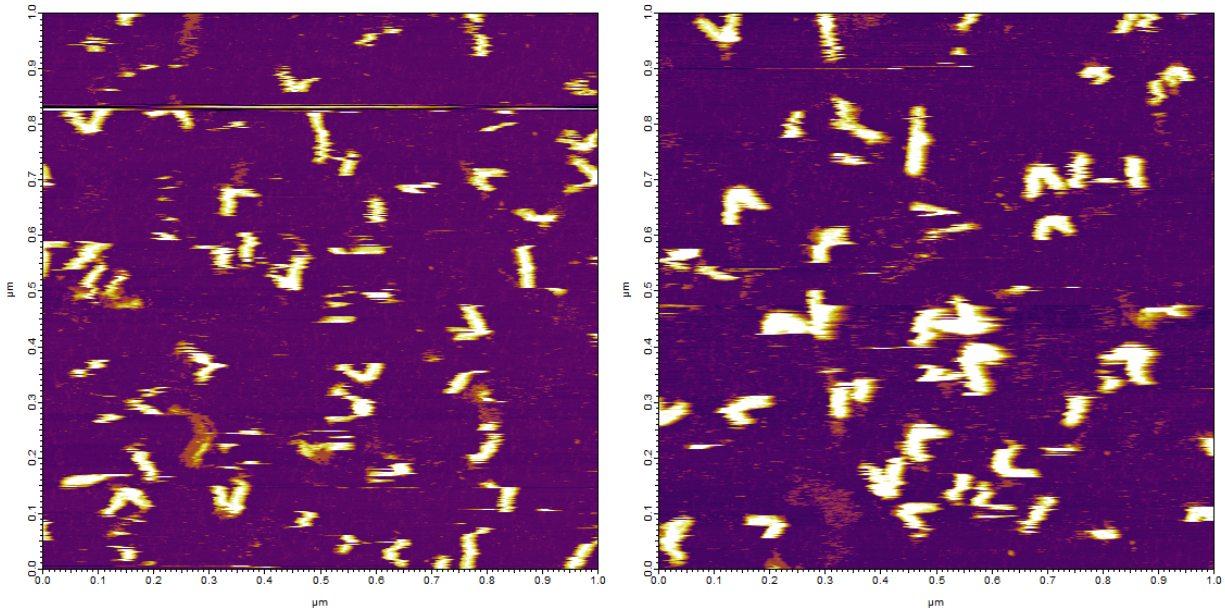

Fig. S6.1: AFM images of the normally closed hinge nanostructure imaged on mica

S7: Cryo-EM Images of Hinge DNA Nanostructures

Below are representative examples of Cryo-EM micrographs of the normally closed hinge nanostructure.

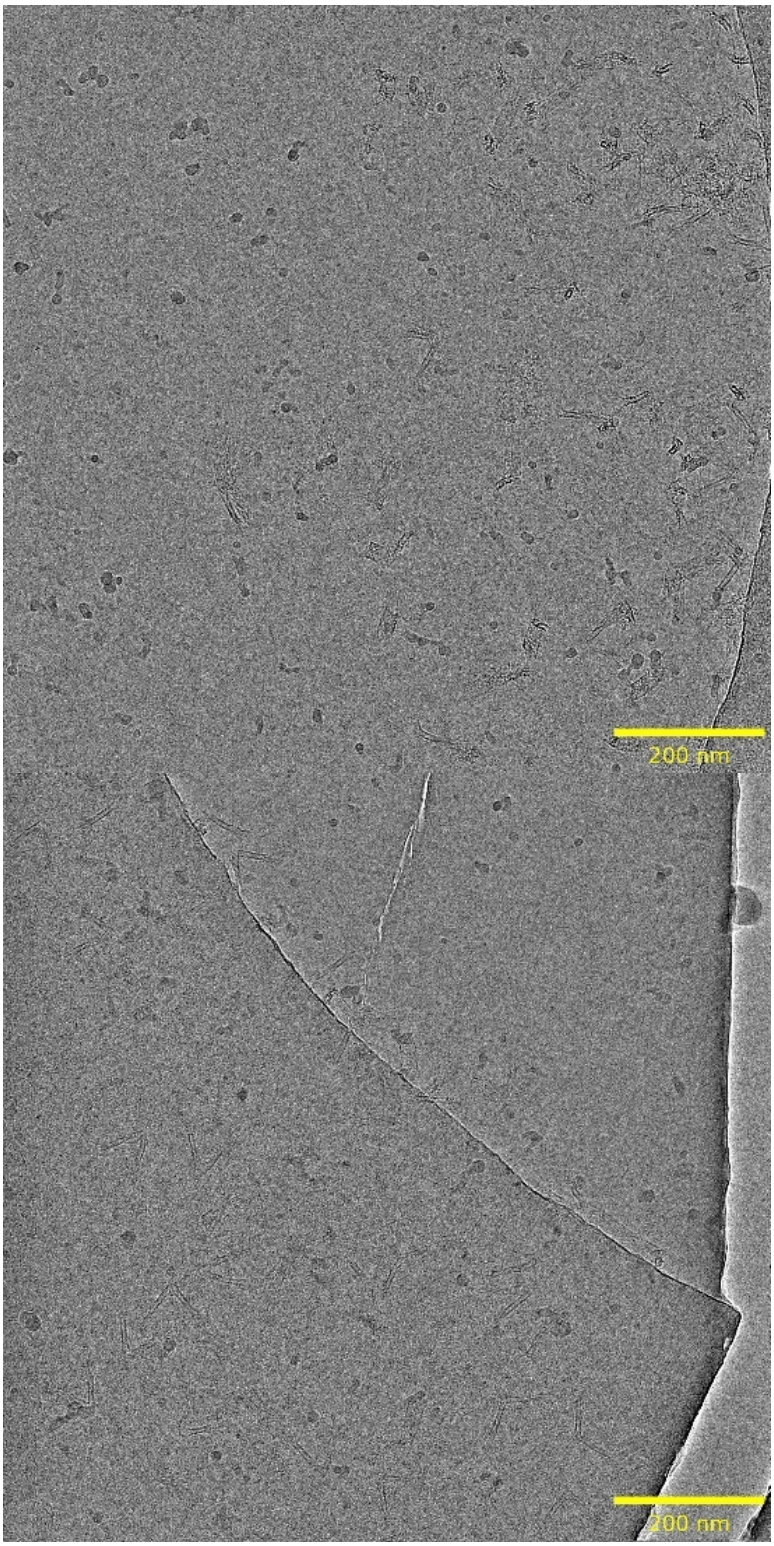

Fig. S7.1: Representative micrographs of the hinge nanostructure

S8: Cryo-EM Methods and 3D Reconstruction

Cryogenic Electron Microscopy measurements were performed using R3.5/1 micromachined holey carbon with 200 mesh copper supports (Quantifoil*) and were glow discharged using a Pelco easiGlow system (25 mA, 25 s glow time, 10 s hold time) prior to sample application. 3 uL of DNA nanostructure solution was applied to the grid by pipetting, then blotted with filter paper for 5.5 s and plunge-frozen into liquid ethane using a Vitrobot (Thermo Fisher Scientific/"TFS"). Microscopy was performed on a Glacios transmission electron microscope (TFS) operated at 200 kV, using a Falcon 4i direct electron detector (TFS). SerialEM[6] was used for automated data collection. Micrographs were collected in Electron Event Representation (EER) mode at a nominal magnification of 57,000x, corresponding to a physical pixel size of 2.49 Å, with an exposure time of 24.98 s and a total dose of 24.8 e/Å^2. Motion correction was performed using Relion v3.1.2[7] with 4K pixel rendering and EER fractionation of 316 frames, corresponding to a dose of 0.987 e/Å^2 per fraction. Roughly 450 particles (hinge halves) were picked manually from a subset of micrographs and extracted using a box size of 200 pixels (498 Å). Extracted particles were subjected to 2D classification in Relion to generate templates, which were then used for automated picking, extraction, and 2D classification of particles from all micrographs. Of the 6,687 total particles, 4,002 particles belonged to classes showing high-resolution features (i.e. DNA helices) and were selected for initial model generation and 3D auto-refinement in Relion. For 2D classification and 3D refinement steps, circular masks of 400 Å were applied, effectively restricting refinement to the central portion of the hinge arm to visualize the arrangement of helices. Masking and postprocessing procedures were then performed within Relion, yielding a final map with a reported resolution of 20 Å.

The 2D class images of the hinge arm prior to 3D reconstruction are given below in Fig. 8.1.

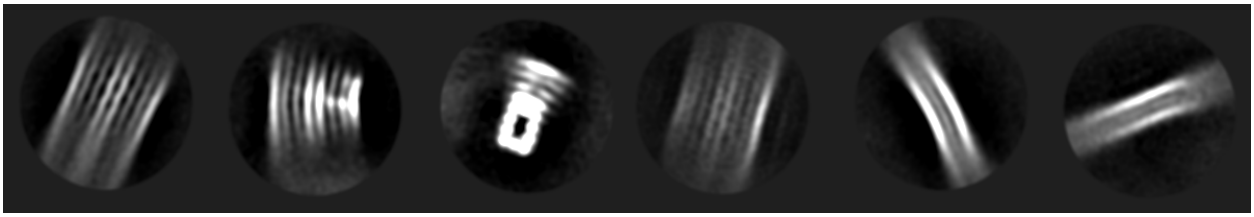

Fig. S8.1: 2D class montage of the hinge arms used to create the 3D reconstruction given in Fig. 1 of the main text.

*Certain commercial equipment, instruments, or materials are identified in this paper to specify the experimental procedure adequately. Such identifications are not intended to imply recommendation or endorsement by the National Institute of Standards and Technology, nor it is intended to imply that the materials or equipment identified are necessarily the best available for the purpose.

S9: Chronocoulometric Measurements to Estimate Surface Density

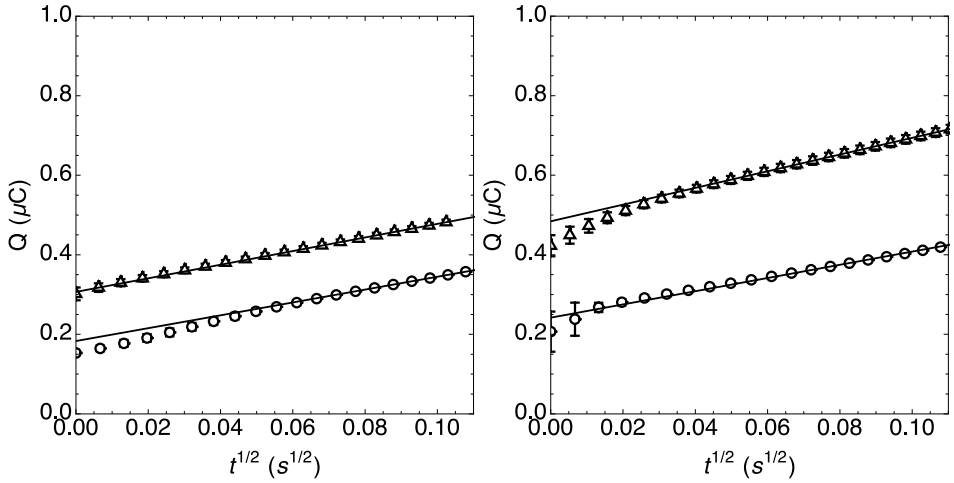

Fig. S9.1: Chronocoulometric response for hybridized dsDNA (*left*) and DNA nanostructure (*right*) in the presence (*triangles*) and absence (*circles*) of 50 μmol/L (μM) of Hexaammineruthenium(III) chloride (RuHex). The solid lines indicate the fit to the data that were used to determine the x-intercept.

Chronocoulometric measurments were used to estimate the surface concentration of both the hybridized dsDNA and the DNA nanostructures following methods in the literature.[8] Fig. S9.1 shows the response curves for each case that was used to estimate the surface concentration[2,8] of each species using the integrated Cottrell equation,

$$Q = \frac{2n\,FAD_0{}^{1/2}C_0}{\pi^{1/2}} t^{1/2} + Q_{dl} + n\,FA\,\Gamma_0 \quad , \qquad \text{(S9.1)}$$

where n is the number of electrons per molecule, F is the Faraday constant, A is the electrode area, D_0 is the diffusion constant, C_0 is the bulk concentration, Q_{dl} is the capacitive charge and $nFA\Gamma_0$ is the charge from the reduction of the adsorbed redox marker. The x-intercept of the lines in Fig. S9.1 include the charge from the electric double layer and the adsorbed redox potential, the difference between the case with and without the redox marker is used to estimate the surface excess of adsorbed marker.

The density of DNA probes (ρ_{DNA}) or DNA nanostructures ($\rho_{Structure}$) on the surface were then determined by,[8]

$$\rho_{DNA}/\rho_{Structure} = \Gamma_0\,(z/m)\,N_a, \qquad \text{(S9.2)}$$

where Γ_0 is computed from Eq. S9.1, z is the charge of the redox molecule, m is the number of bases and N_a is Avogadro's number.

S10: Surface Regeneration and Signal to Noise Ratio

The limit of detection (LOD) was determined by first calculating the signal-to-noise ratio (SNR) of the change in capacitance for each structure using the expression $S=20\log_{10}(\Delta C)$. The SNR was then plotted against the measured analyte concentration as seen from Fig. S10.1 The LOD was estimated by extrapolating the SNR to the noise floor at 10 dB.

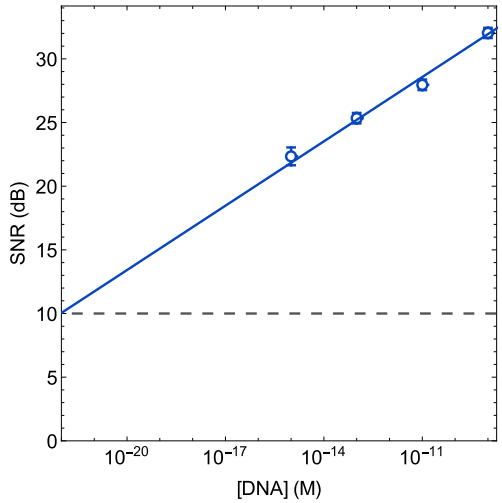

Fig. S10.1: Signal-to-noise ratio of the measured capacitance as a function of analyte concentration in solution

The measurement chip was regenerated by using an antidote DNA sequence that utilizes strand displacement to remove any bound analyte and reset the measurement. This is apparent from Fig. S10.2 where the antidote strand returns the capacitance to its baseline value after each analyte concentration is measured.

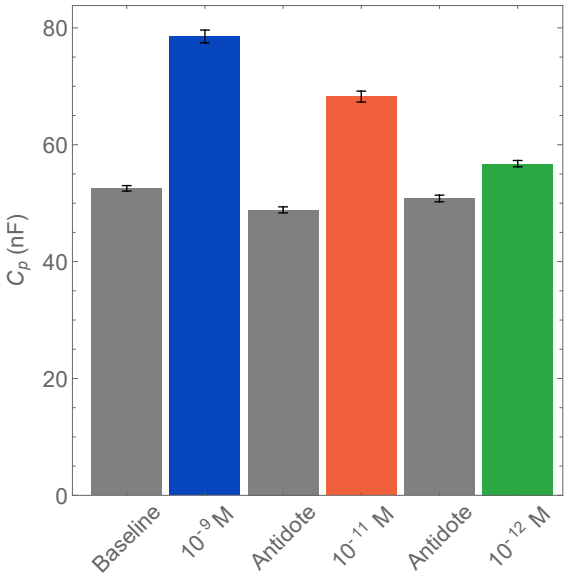

Fig. S10.2: Surface regeneration with an antidote strand allowed a return to the baseline capacitance to allow the chip to be reused for multiple measurements.

S11: Modifying Electrodes with DNA Origami

To verify the attachment of DNA origami to the surface, we measured the capacitance of the electrode as a function of time at a frequency, F=100 Hz. At time, t=0 s the measured capacitance was found to be consistent with that of the electric double layer formed on a bare gold ≈120 nF (15 μF/cm^2) assuming an electrode diameter of 1 mm.[9] As the DNA origami adsorbed to the surface the capacitance fell dramatically to ≈30 nF (4 μF/cm^2). The original capacitance was not recovered after washing the electrode multiple times. Furthermore, non-specific adsorption was tested with a non-thiolated DNA sequence, which resulted in a decrease in the capacitance. This surface was non-responsive to both analyte and applied electric field.

Fig. S11.1: Dynamic response of the capacitance as a function of time. DNA origami was injected into the fluid cell at time, t=0 s. Measurements were made at a constant frequency, F=100 Hz. The curve shows one representative example of the measurement of the surface modification in real-time.

References

1. Darcy, M. *et al.* High-Force Application by a Nanoscale DNA Force Spectrometer. *ACS Nano* **16**, 5682–5695 (2022).
2. Bard, Allen J. & Faulkner, Larry R. *Electrochemical Methods: Fundamentals and Applications*. (Wiley, 2000).
3. Wang, L. *et al.* A sensitive DNA capacitive biosensor using interdigitated electrodes. *Biosens. Bioelectron.* **87**, 646–653 (2017).
4. Oldham, K. B. A Gouy–Chapman–Stern model of the double layer at a (metal)/(ionic liquid) interface. *J. Electroanal. Chem.* **613**, 131–138 (2008).
5. Doblhoff-Dier, K. & Koper, M. T. M. Modeling the Gouy–Chapman Diffuse Capacitance with Attractive Ion–Surface Interaction. *J. Phys. Chem. C* **125**, 16664–16673 (2021).
6. Schorb, M., Haberbosch, I., Hagen, W. J. H., Schwab, Y. & Mastronarde, D. N. Software tools for automated transmission electron microscopy. *Nat. Methods* **16**, 471–477 (2019).
7. Zivanov, J. *et al.* New tools for automated high-resolution cryo-EM structure determination in RELION-3. *eLife* **7**, e42166 (2018).
8. Steel, A. B., Herne, T. M. & Tarlov, M. J. Electrochemical Quantitation of DNA Immobilized on Gold. *Anal. Chem.* **70**, 4670–4677 (1998).
9. López-García, J. J., Horno, J. & Grosse, C. Differential capacitance of the diffuse double layer at electrode-electrolyte interfaces considering ions as dielectric spheres: Part I. Binary electrolyte solutions. *J. Colloid Interface Sci.* **496**, 531–539 (2017).